JOURNAL OF SOLID STATE CHEMISTRY 56, 269–277 (1985)

Photoelectrochemical Properties of Zinc Oxide Doped with 3*d* Elements

M. JAKANI, G. CAMPET, J. CLAVERIE

Laboratoire de Chimie du Solide du CNRS, Université de Bordeaux I, 351 cours de la Libération - 33405 Talence Cedex, France

AND D. FICHOU, J. POULIQUEN, AND J. KOSSANYI

Laboratoire de Photochimie Solaire, ER 241 du CNRS, 2-8 rue Henry Dunant - 94320 Thiais, France

Received May 11, 1984; in revised form July 25, 1984

The properties of ZnO photoanodes doped with transition elements (Cr, Mn, Fe, Co, Ni) have been investigated for photodecomposition of aqueous solutions. A large extension of the photoresponse occurs in the visible region, particularly with Co^{2+}- and Mn^{2+}-doped samples. The doping-ion coordination, the energy levels, and the mechanism of the charge transfer are discussed. © 1985 Academic Press, Inc.

Introduction

Semiconducting metal oxides used as photoanodes in the decomposition of water are found to be the most stable materials toward photocorrosion in aqueous medium. Unfortunately their efficiency is very low in solar energy conversion since their band gap is rather large ($E_g \simeq 3.2$ eV). Using TiO_2 and $SrTiO_3$ oxides, the doping with 3*d* elements has been found to induce, in the visible region of the solar spectra, photoactive transitions between d^n ions and the titanium conduction band. These doping agents generally form intraband-gap localized levels and act as traps for most of the generated photoelectrons, thus inhibiting drastically the intensity of the photocurrent. However, three of us have shown in a recent paper that such materials give a net photocurrent provided that the conduction band is large enough to favor an effective charge transfer (*1–3*).

Most of the transition metal oxides have a narrow conduction band associated to 3*d* orbitals. Nevertheless, as far as ZnO is concerned, the Zn : 3*d* orbitals are filled and form the valence band together with the O : 2*p* orbitals; thus, the conduction band, which arises from the Zn : 4*s* orbitals, should be large; consequently it is expected that it will induce a high electron mobility, making possible an efficient electron-hole separation, even if the holes are generated in narrow doping levels. Besides this, the wurtzite-type structure of ZnO exhibits a large amount of native defects: one of them, interstitial zinc, gives donor levels which lie close to the conduction band and, as a consequence, make ZnO a *n*-type semiconductor (*4*). Although zinc oxide is lightly unstable under illumination (*5, 6*), it should

0022-4596/85 $3.00

induce the photoelectrolysis of water since the Zn : 4*s* conduction band edge is localized near the H^+/H_2 level and the valence band edge below the O_2/H_2O level. However, because of its quite large band gap (E_g = 3.2 eV) many attempts to sensitize ZnO to visible light have been successful using dyes adsorbed at the surface of the semiconductor (*7–10*) or dissolved in the electrolyte (*11–13*); but the efficiency of these systems has been found to be rather low.

The goal of the present article is to investigate the photoresponse of polycrystalline *n*-type zinc oxide semiconductors doped with several 3*d* cations, and to propose tentatively a model which can account for the resulting photoelectrochemical properties.

As it has been already pointed out, an efficient conversion of the solar energy implies that the 3*d* cations introduced in the wurtzite lattice takes place in the same tetrahedral surrounding as the Zn^{2+} ions to which they have been substituted (*14, 15*).

Large number of ions can be introduced in the zinc oxide lattice but several of them are likely to be reduced by Zn^+ donor centers which normally confer a *n*-type character.

These considerations imply necessarily that only Cr^{3+}, Mn^{2+}, Fe^{3+}, Co^{2+}, and Ni^{2+} can be stabilized in the *n*-ZnO lattice. On the other hand it is known that the ground state of Cu^{2+} is localized near the conduction band of ZnO, and, thus, can hardly give rise to a visible photoresponse (*16*).

The solubility of NiO in ZnO is about 1%—in order to facilitate the comparison of the behavior of the various materials, they have all been doped with the same amount of 3*d* elements (*1% in atoms*).

I. Experimental

The compounds have been prepared by grinding intimately in an agate mortar finely divided powders of the dehydrated reactants. Then they have been pelletized under 3 tons pressure and sintered at 1300°C for 15 hr.

The electrodes were prepared following the same procedure as the one described previously (*1*). The electric contact was made by soldering an ohmic In/Ga alloy on one side of the sintered pellets.

The electrochemical measurements have been carried out using a "three-electrode device": the active electrode, a platinum counterelectrode, and a saturated calomel electrode (SCE). The electrolyte used is 1 *M* NaOH solution. Electrode potentials are measured versus the SCE using a Tacussel PRT 20 – 2X type potentiostat. Photocurrents are measured under the output of a 150-W xenon lamp and corrected for the quantum flux of the light source.

Optical measurements have been carried out with a CARY 17 type spectrometer. Absorption spectra have been obtained by the diffuse reflectance technique.

ESR spectra have been obtained using a ER 200 tt spectrometer.

II. Results and Discussion

1. X-Ray and ESR Analysis

The X-ray diffraction diagrams indicate that when they are prepared at 1300°C for 15 hr, all the doped ZnO samples have a wurtzite-type structure.

The oxidation numbers and the crystallographic sites of the dopant have been determined when it is possible by ESR and absorption spectra. ESR spectrum of ZnO : Cr carried out at room temperature characterizes the chromium at the trivalent state: the *g* value (1.964) indicates that Cr^{3+} is localized in the octahedral site.

Figure 1 shows the ESR signal of ZnO : Mn recorded at room temperature. This spectrum gives a value of g = 2.02 which characterizes the presence of Mn^{2+} ion whatever the oxidation number of the

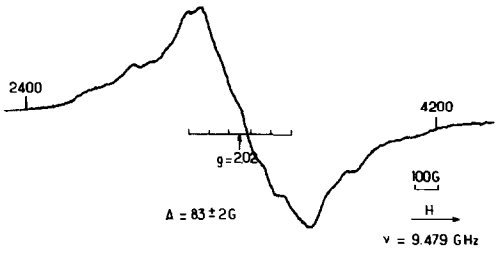

FIG. 1. ESR spectrum of ZnO doped with Mn^{2+}.

Mn introduced may be. The six hyperfine lines observed are due to the nuclear spin $I = 5/2$ of the manganese.

The ESR spectrum of ZnO : Fe exhibits a $g = 4.28$ G value correlated to Fe^{3+} ion. Since both Mn^{2+} and Fe^{3+} ions have an $I = 5/2$ nuclear spin the ESR spectroscopy cannot bring any information about the site symmetry.

In spite of the lack of any ESR signal from the Co^{2+} and Ni^{2+} ions, a tetrahedral or octahedral coordination may be postulated for them in the ZnO lattice on the basis of the following two reasons:

(i) The spin–lattice relaxation time for Co^{2+} ions in an octahedral surrounding is very short and the corresponding ESR signal can be observed only at liquid-helium temperature. As a matter of fact, several authors (*17*) have observed that the hyperfine splitting expected from Co^{2+}_{oct} ($I = 7/2$) is unresolved even at liquid-helium temperature. Furthermore, the signal ascribed to CO^{2+}_{oct} vanishes whereas that resulting from the lattice defects are still observed when the temperature increases.

(ii) Octahedrally coordinated Ni^{2+} signal has not been observed and, on the other hand, no ESR signal has been claimed yet for tetrahedrally coordinated $Ni^{2+}(e^4_g t^4_{2g})$. Consequently, the identification of these two ions in the ZnO lattice is made impossible on the sole basis of ESR spectroscopy. As described hereunder this attribution can be made from the absorption spectra.

2. *Optical Absorption*

The absorption spectra of doped ZnO are depicted on Fig. 2. The main absorption of *n*-ZnO sintered samples is observed around 380 nm; it does not drop sharply but rather shows a long tail which goes up to 700 nm. This tailing band can undoubtedly be correlated to the defects introduced by thermal treatment for making ZnO a *n*-type semiconductor.

The $ZnO : Cr^{3+}$ spectrum shows two broad absorption bands centered at about 580 and 660 nm. According to the octahedral symmetry of Cr^{3+} ions, the latter a weak and diffuse band, could be attributed to a spin-forbidden d–d transition $^4A_2 \rightarrow {}^2T_1$ while the former is due to the spin-allowed $^4A_2 \rightarrow {}^4T_2$ transition. A second expected spin-allowed transition $^4A_2 \rightarrow {}^4T_1$ might appear at higher energy and thus it is hidden by the $O : 2p \rightarrow Zn : 4s$ charge-transfer band.

Both Mn^{2+} and Fe^{3+} ions having the same d^5 high-spin electronic configuration, any d–d transition (spin-forbidden) can be expected. As a consequence the main absorp-

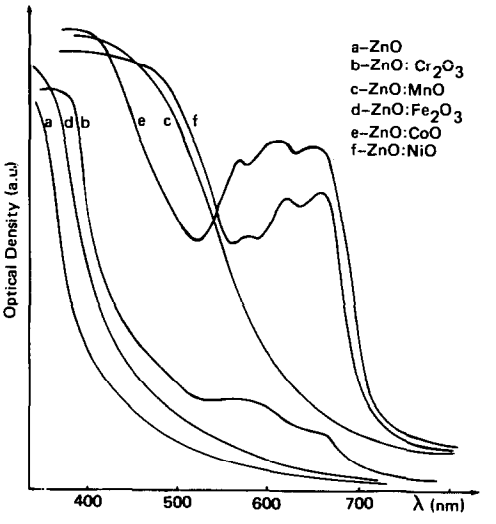

FIG. 2. Absorption spectra of normally undoped and doped ZnO samples.

tion of the corresponding $ZnO:Mn^{2+}$ and $ZnO:Fe^{3+}$ samples exhibit the same charge-transfer band as pure ZnO. However, regarding $ZnO:Mn^{2+}$ the results obtained by photoacoustic spectroscopy (*18*) show clearly the characteristic bands of tetrahedrally coordinated Mn^{2+} ions which can be associated to the ${}^6A_1 - {}^4T_2$ transition at 380 and 420 nm as already described by Bates *et al.* (*19*); here again, a long tail is observed which extends the absorption to the red. A rather broad band is found for $ZnO:Co^{2+}$ which is between 500 and 700 nm and which can be attributed to the ${}^4A_2 \rightarrow {}^4T_1$ transition. The strong spin–orbit coupling splits the ${}^4T_1$ state into three energy levels leading to structured band with peaks at 560, 620, and 650 nm (*20, 21*).

Similarly, the $ZnO:Ni^{2+}$ sample exhibits a large absorption band corresponding to the ${}^3T_1(F) \rightarrow {}^3T_1(P)$ transition with three peaks localized at 570, 630, and 660 nm (*21*).

According to Weakliem (*22*) these absorption spectra obtained at room temperature are typical of a tetrahedral coordination of Co^{2+} and Ni^{2+} ions.

3. Flatband Potentials and Mott–Schottky Plots

The photocurrent–voltage curves shown on Fig. 3 give evidence for the *n*-type character of the investigated samples. Compared to the −0.9-V value obtained for undoped ZnO, the photocurrent onset potential is found more anodic for the doped samples, with a deviation which can reach 0.3 V in the case of the $ZnO:Ni^{2+}$ electrode, although the electronegativity of the dopants are near to that of zinc.

The space charge capacities C_{sc} have been determined in the dark from impedance measurements following the procedure described by Tomkiewicz (*23*) and assuming no additional capacitance introduced by surface states. Figure 4 shows the linear variations of C_{sc}^{-2} versus the applied potential obtained for ZnO undoped and doped by Mn, Co, or Ni. These lines intercept the potential axis at a poten-

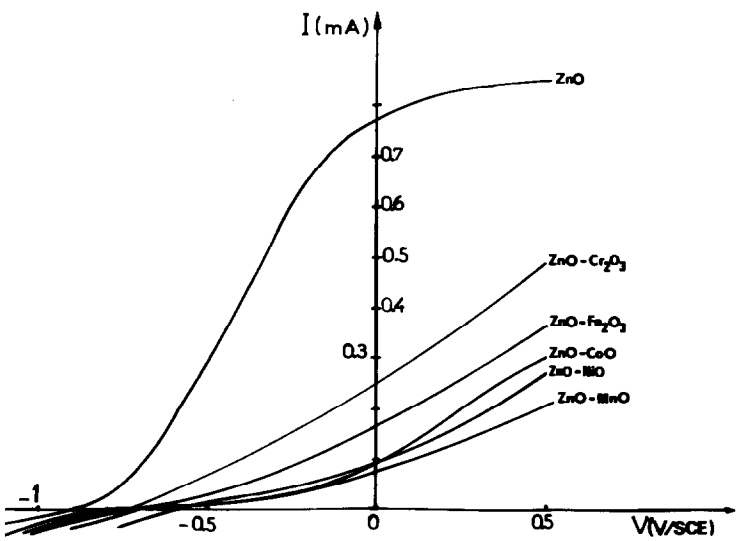

FIG. 3. Photocurrent potential curves obtained under full light illumination of the semiconducting electrodes at pH 13.

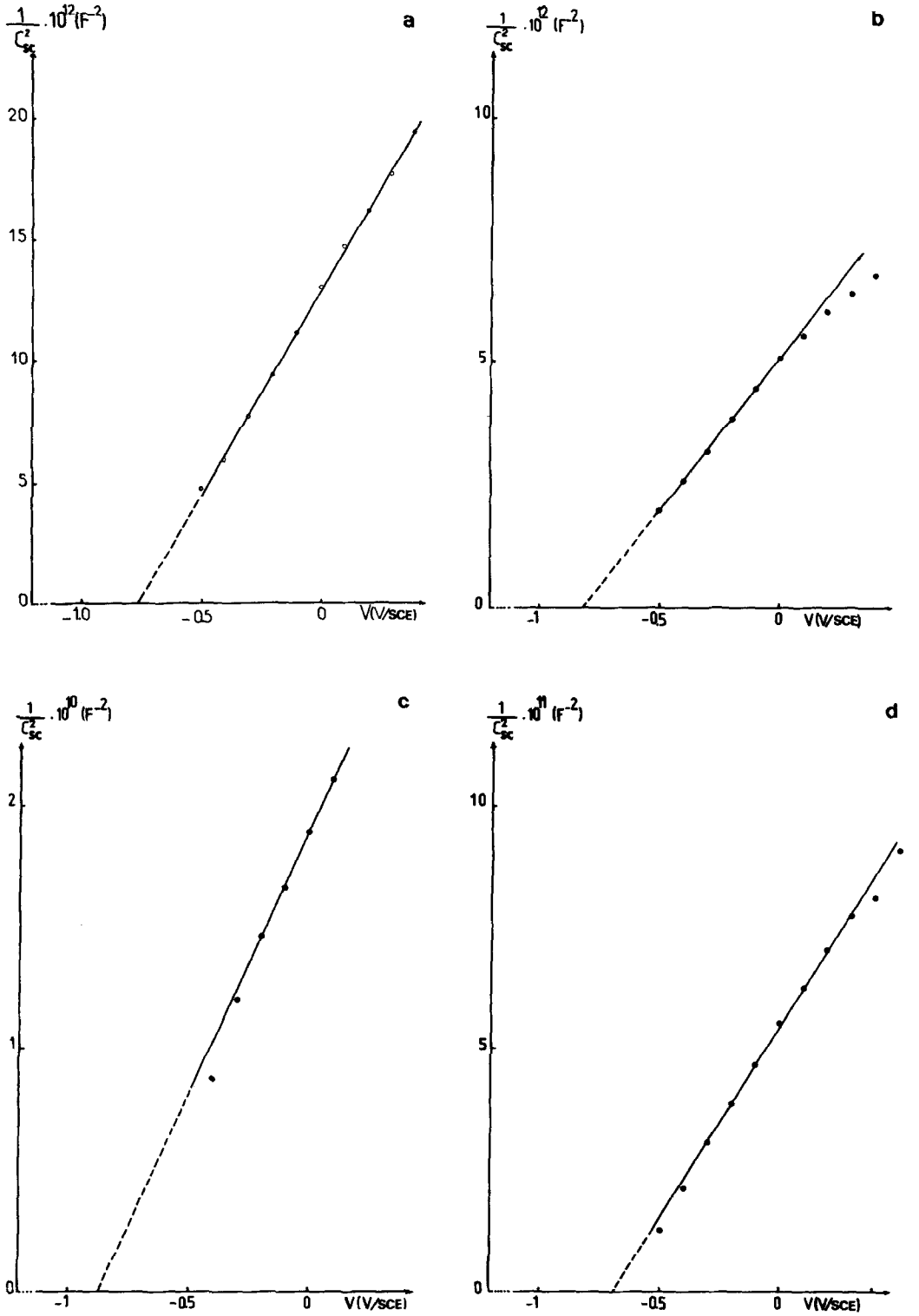

FIG. 4. Mott–Schottky plots at pH 13 and 1 kHz of (a) ZnO, (b) ZnO : Mn^{2+}, (c) ZnO : Co^{2+}, (d) ZnO : Ni^{2+}.

tial value which agrees with the V_{fb} measured from the photocurrent variation. The values of the free charge carrier concentration N_D, calculated from the slope of the straight lines, are listed in Table I together with the main characteristics of the studied samples.

4. Action Spectra

Figure 5 shows the photoresponse as a function of the excitation wavelength with a potential of 0 V/SCE applied to the doped ZnO electrodes.

As expected, no sensitization to the visible is accounted for the Fe^{3+}-doped sample, but a large one extending far into the visible region is observed for the other doped semiconductors (up to 700 nm for Mn^{2+} and 750 nm for Co^{2+}).

All anodes, $ZnO:Ni^{2+}$ excepted, exhibit a variation of the photocurrent similar to that of the optical absorption. With $ZnO:Ni^{2+}$, no photocurrent is observed above 620 nm, although a large absorption band, attributed to the $^3T_1(F) \rightarrow {}^3T_1(P)$ transition, occurs between 550 and 700 nm. Thus, it can be assessed that the $^3T_1(P)$ levels are localized inside the band gap; the onset at 550 nm for the photocurrent and the maximum at 500 nm could be associated to a $Ni^{2+}(t_{2g}^4) \rightarrow Zn^{2+}(4s^\circ)$ charge transfer.

5. Energy Levels and Charge Transfer Mechanisms

The photocurrent in the visible region can reasonably be associated with an electronic charge-transfer between the $3d^n$ levels and the conduction band. The holes photogenerated must have a mobility large enough to move toward the electrode/electrolyte interface in order to oxidize water and yield the evolution of oxygen. A weak enough anodic bias would contribute to a tunneling effect of the holes into the valence band and to an increase of the corresponding photocurrent. Then the position of the $3d^n$ levels can be estimated for each doped electrode from the onset of the photocurrent (Fig. 6a).

Cr^{3+} and Ni^{2+} constitute narrow bands lying about 2.2 eV below the bottom of the conduction band.

Concerning the $ZnO:Mn^{2+}$ and $ZnO:Co^{2+}$ anodes we can deduce from their large photoresponse, which extends down to 700 nm (1.8 eV) and 750 nm (1.65 eV), respectively, that the $Mn^{2+}(t_{2g}^3)$ and $Co^{2+}(t_{2g}^4)$ states lie approximately in the middle of the band gap. Due to this particular situation, the above described mechanism might be inadequate and we can put forward two different mechanisms to take into account for the observed photocurrent:

(i) An electronic transition from the valence band of ZnO to the subband gap

TABLE I

MAIN CHARACTERISTICS OF THE INVESTIGATED SAMPLES

	σ ($\Omega^{-1}cm^{-1}$)	N_D (cm^{-3})	μ_e ($cm^2/v.s.$)	Energy onset of the photocurrent (eV)	V_{fb} from Onset potential (V/SCE)	V_{fb} from Mott–Schottky plots (V/SCE)
ZnO	1	9.7×10^{18}	0.640	3.20 (E_g)	−0.90	−0.80
$ZnO:Cr^{3+}$	5×10^{-2}	—	—	2.20	−0.75	—
$ZnO:Mn^{2+}$	10^{-1}	3.3×10^{19}	0.020	1.80	−0.75	−0.80
$ZnO:Fe^{3+}$	3×10^{-2}	—	—	2.75	−0.70	—
$ZnO:Co^{2+}$	10^{-1}	1.1×10^{20}	0.006	1.65	−0.90	−0.90
$ZnO:Ni^{2+}$	10^{-1}	2.4×10^{20}	~0.003	2.10	−0.60	−0.70

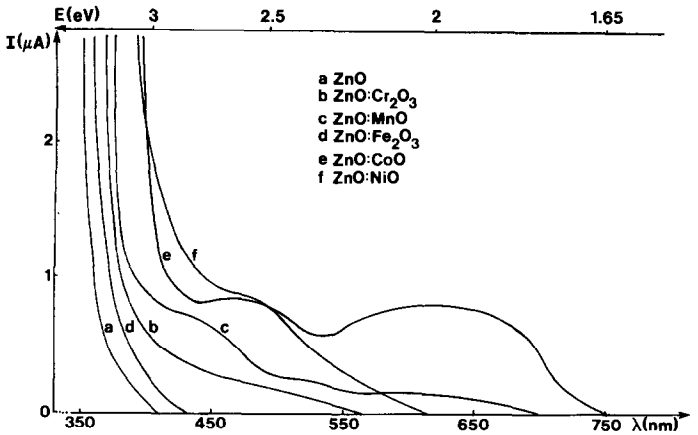

FIG. 5. Action spectra of the semiconducting electrodes at pH 13 and under a $V = 0$ V/SCE anodic bias.

states (Mn^{2+} or Co^{2+}), followed by an electron tunneling to the conduction band; the corresponding photoholes are generated in the valence band and can easily reach the surface of the electrode (Fig. 6b). But these Mn^{2+} and Co^{2+} levels must be empty in order to act as acceptor states for the electrons photoexcited. Then the Fermi level must be lowered below the impurity states by a large anodic bias (>1.55 V for Co^{2+}).

(ii) An electronic transition from the intraband gap states (Mn^{2+} and Co^{2+}) into the conduction band of ZnO as pointed out previously (Fig. 6c). In this mechanism, either a large anodic bias must be applied to the electrode in order to instigate a hole tunneling effect via the valence band (>1.4 V for Mn^{2+} and >1.55 V for Co^{2+}) or the holes migrate in the impurity band toward the surface of the electrode, with a high mobility.

As shown in Fig. 5, a net photocurrent is observed when the potential applied to the electrode is low: $V = 0.8$ V (i.e., 0.0 V/SCE). Then neither the mechanism (i) nor the hole tunneling effect in mechanism (ii) are likely to occur. As a consequence mechanism (ii) could be taken into account provided the hole mobility in the subband gap states is enhanced by an appropriate phenomenon (such as structure defects, impurity levels, etc.) in order to cross the depletion layer and reach the surface of the electrode (Fig. 6d).

This could result from a concentration gradient of the dopant near the surface of the electrode enlarging the narrow impurity band or increasing the number of surface states within the band gap.[1] Such a possibility cannot be neglected since the same photoresponse has been found for an electrode doped with cobalt by two different ways:

—Sintering at 1200°C a pellet prepared from an intimate mixture of ZnO and CoO.

—Introducing Co^{2+} inside a presintered ZnO pellet by evaporation of Co_3O_4 in aerated atmosphere (*17*).

A slight difference in concentration, larger at the surface than in the bulk has been claimed already for $Zn_{0.99}Co_{0.01}O$ pellets (*24*).

We can notice that the onset of $ZnO:Mn^{2+}$ and $ZnO:Ni^{2+}$ anodes occurs at 700 and 600 nm, respectively. These values are shifted toward the long wavelengths as compared to the onsets of the $TiO_2:Mn^{2+}$ (430 nm) and $TiO_2:Ni^{2+}$ (550 nm) electrodes (*1*).

[1] Such an hypothesis is under investigation and will be published later.

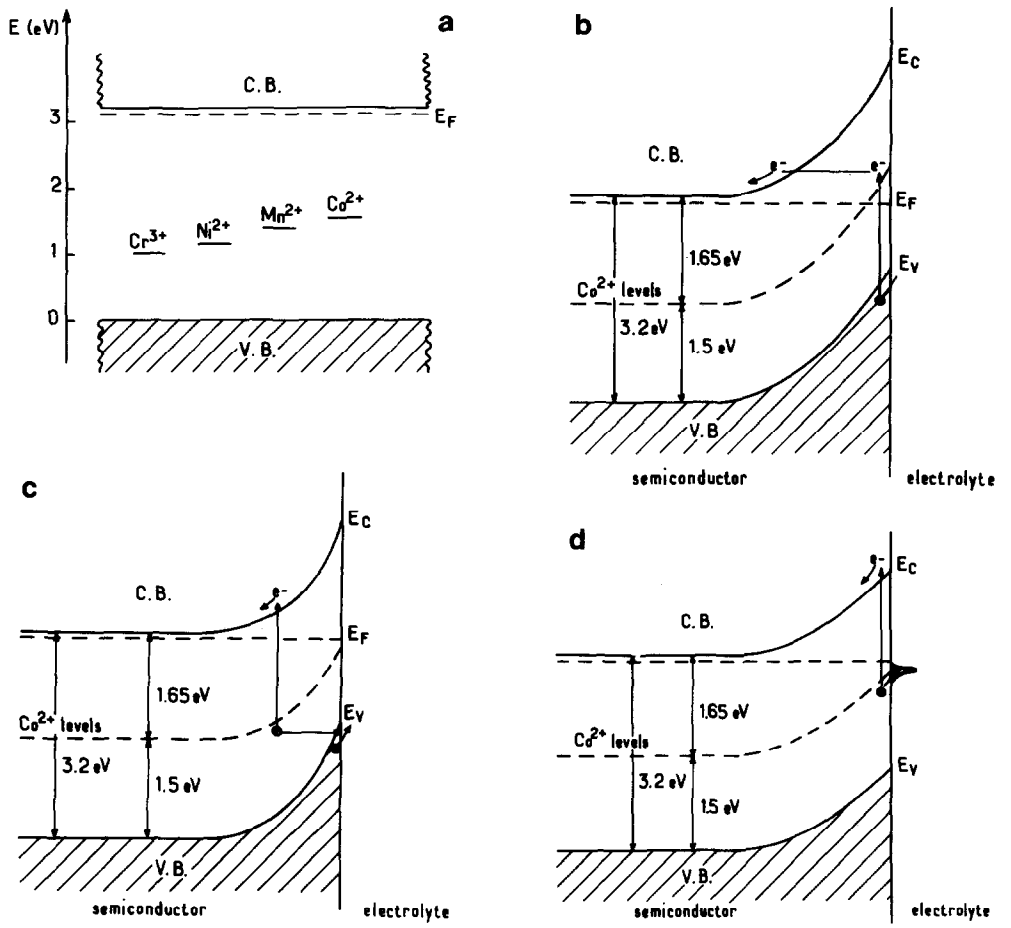

FIG. 6. Impurity levels in doped ZnO samples and possible processes giving rise to a visible photoresponse: (a) impurity levels, (b) mechanism (i), (c) mechanism (ii), (d) most likely mechanism.

If one assumes that the TiO_2 and ZnO valence bands, which arise both from the $2p$ oxygen orbitals, lie at the same level and that the band gaps have identical widths (3.2 eV), then the previous values give evidence that the electron–hole recombination is higher in the doped TiO_2 electrodes than in the analogously doped ZnO electrodes. This result is consistent with the high mobility of the electrons expected in the large ($4s$, $4p$) zinc oxide conduction band.

Acknowledgments

The authors thank J. M. Dance for the ESR spectroscopy measurements as well as for helpful interpretation and C. Parent for fruitful discussions.

References

1. G. CAMPET, J. VERNIOLLE, J. P. DOUMERC, AND J. CLAVERIE, *Mater. Res. Bull.* **15,** 1135 (1980).
2. J. CLAVERIE, J. VERNIOLLE, G. CAMPET, J. P. DOUMERC, AND P. HAGENMULLER, *Mater. Res. Bull.* **16,** 1019 (1981).
3. G. CAMPET, M. JAKANI, J. P. DOUMERC, J. CLAVERIE, AND P. HAGENMULLER, *Solid State Commun.* **42,** 93 (1982).
4. P. KOFSTAD, "Nonstoichiometry, Diffusion, and Electrical Conductivity, in Binary Oxides." Wiley–Interscience, New York (1972).
5. G. PETERMANN, H. TRIBUTSCH, AND BOGOMOLNI, *J. Chem. Phys.* **57,** 1026 (1972).
6. H. GERISCHER, *J. Electrochem. Soc.* **113,** 1174 (1966).
7. E. MICHEL-BEYERLE, H. GERISCHER, F. REBEN-

TROST AND M. TRIBUTSCH, *Electrochim. Acta* **13,** 1509 (1968).
8. M. MATSUMURA, S. MATSUDAIRA, AND H. TSUBOMURA, *Eng. Chem. Prod. Res. Dev.* **19,** 415 (1980).
9. J. NASIELSKI, A. KIRSCH, AND P. LEEMPOEL, *Electrochim. Acta* **23,** 605 (1978).
10. D. MAUREL, J. POULIQUEN, D. FICHOU, J. KOSSANYI, AND M. LE LIBOU, in press.
11. M. DE BACKER, M. C. RICHOUX, F. LE CLERCQ, AND G. LEPOUTRE, *Rev. Phys. Appl.* **15,** 529 (1980).
12. T. SAKATA, Y. SUDA, J. TANAKA, AND H. TSUBOMURA, *J. Phys. Chem.* **81,** 537 (1977).
13. N. ALONSO, M. BELLEY, P. CHARTIER, AND V. ERN, *Rev. Phys. Appl.* **16,** 5 (1981).
14. R. PAPPALARDO, D. L. WOOD, AND R. C. LINARES, JR., *J. Chem. Phys.* **35,** 1460 (1961).
15. F. PEPE, M. SCHIAVELLO, AND G. FERRERIS, *J. Solid State Chem.* **12,** 63 (1975).
16. E. MOLLWO, G. MULLER, AND P. WAGNER, *Solid State Commun.* **13,** 1283 (1973).
17. K. DYREK AND Z. SOJKA, *J. Chem. Soc. Faraday Trans.* **78,** 3177 (1981).
18. D. FICHOU, J. POULIQUEN, AND J. KOSSANYI, submitted for publication.
19. C. H. BATES, W. B. WHITE, AND R. ROY, *J. Inorg. Nucl. Chem.* **28,** 397 (1966).
20. V. GOMATHY, C. BASU, AND U. S. GOSH, *Phys. Status Solidi B* **86,** 379 (1978).
21. R. S. ANDERSON, *Phys. Rev.* **164,** 398 (1967).
22. H. A. WEAKLIEM, *J. Chem. Phys.* **36,** 2117 (1962).
23. M. TOMKIEWICZ, *J. Electrochem. Soc.* **126,** 2220 (1979).
24. B. TANOUTI, J. P. BONNET, R. SALMON, AND M. ONILLON, *Mater. Lett.* **1,** 73 (1982).